

Interfacial Decoupling Layer Enabled Low-*n* Phase Enrichment for Blue Quasi-2D Perovskites

Jie Dong, Wenqiang Yang, Kayoung Cho, Jeong Hyun Jung, Huanyu Zhou, Eojin Yoon, Hao Chen, Hyeon-Dong Lee, Seung Hyeon Jo, Jae-Man Park, Qingsen Zeng, Tingyu Long, Kyung Yeon Jang, Seong Eui Chang, Chan-Yul Park, Min-Jun Sung, Joo Sung Kim, Hyeree Kim, Dandan Song, Zheng Xu, JaeHong Park, Jeong-Yun Sun, and Tae-Woo Lee*

Cite This: *ACS Energy Lett.* 2024, 9, 5879–5887

Read Online

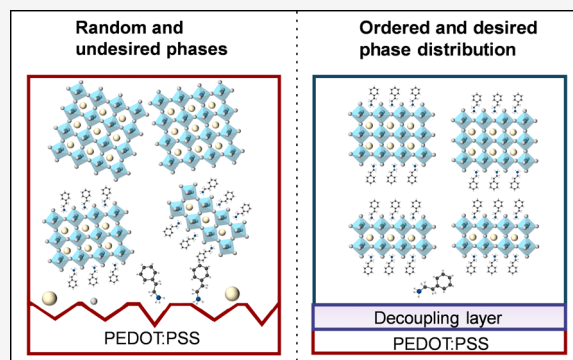
ACCESS |

Metrics & More

Article Recommendations

Supporting Information

ABSTRACT: The random *n*-monolayer phase distributions and impurity phases impose challenges to achieving blue-emission quasi-2D perovskite light emitting diodes (PeLEDs), and their formation mechanism is unclear. Here, we uncover the reasons behind the phase formation and distribution in blue-emission quasi-2D perovskites by probing into the molecular interactions at the buried interface between substrates and perovskites and propose a mechanistic model to depict the film formation process. Furthermore, an interfacial decoupling layer, perfluorinated ionomer, was employed to successfully mitigate the negative impact of substrates on the phase formation and distribution of blue-emission quasi-2D perovskites, resulting in an ordered phase distribution and a reduction of undesired phases. Besides, this interfacial layer effectively suppressed the nonradiative recombination losses, leading to enhanced photoluminescence quantum yield from 12.71% to 60.13% and notable blue shift (~10 nm) even without incorporating Cl ions. As a result, blue PeLEDs based on this strategy achieved an external quantum efficiency reaching 12.09%.



Quasi-two-dimensional (quasi-2D) perovskites present great potential for next-generation full-color display, owing to their tunable bandgap, high color purity, wide color gamut, and low cost. Their general chemical formula can be represented as $L_2A_{n-1}B_nX_{3n+1}$, where L stands for large organic cations, A is small cations, B represents metal cations, and X is a halide ion. The key parameter *n* represents the number of inorganic octahedral monolayers $[PbX_6]^{4-}$ sandwiched between the organic spacer layers, thus forming quantum wells (QWs). Especially, quasi-2D perovskites have emerged as a focal point in blue-emission perovskite light emitting diodes (PeLEDs).^{1,2} However, the existence of large cations in blue quasi-2D perovskites primarily tends to form high-energy phases, complicating the crystallization process and hindering precise control of *n*-monolayer phases (hereafter, *n*-phases). Uncontrollable crystallization causes nonuniform grain size and morphology, alongside defects like dislocations and impurities, consequently degrading stability and reproducibility. Most critically, it causes issues on precise management of their orientation and phase

distribution in 2D perovskite materials, which is crucial for promoting color purity and efficiency of blue emitting PeLEDs.

The current strategies to address these issues mainly involve complicated control over the 2D-spacer cation engineering,^{3–6} dopants^{7,8} or preparation conditions.^{9,10} Despite these advancements, the synthesis of high-quality blue-emission quasi-2D perovskites remains sensitive to environmental factors. This should be due to the unclear phase formation mechanism and the underexplored interaction at the buried interface between the substrate and quasi-2D perovskites. To address these challenges, the buried interface has become a key focus owing to its important role in controlling phase distribution and purity, directly impacting perovskite film

Received: August 26, 2024

Revised: November 6, 2024

Accepted: November 6, 2024

Published: November 18, 2024

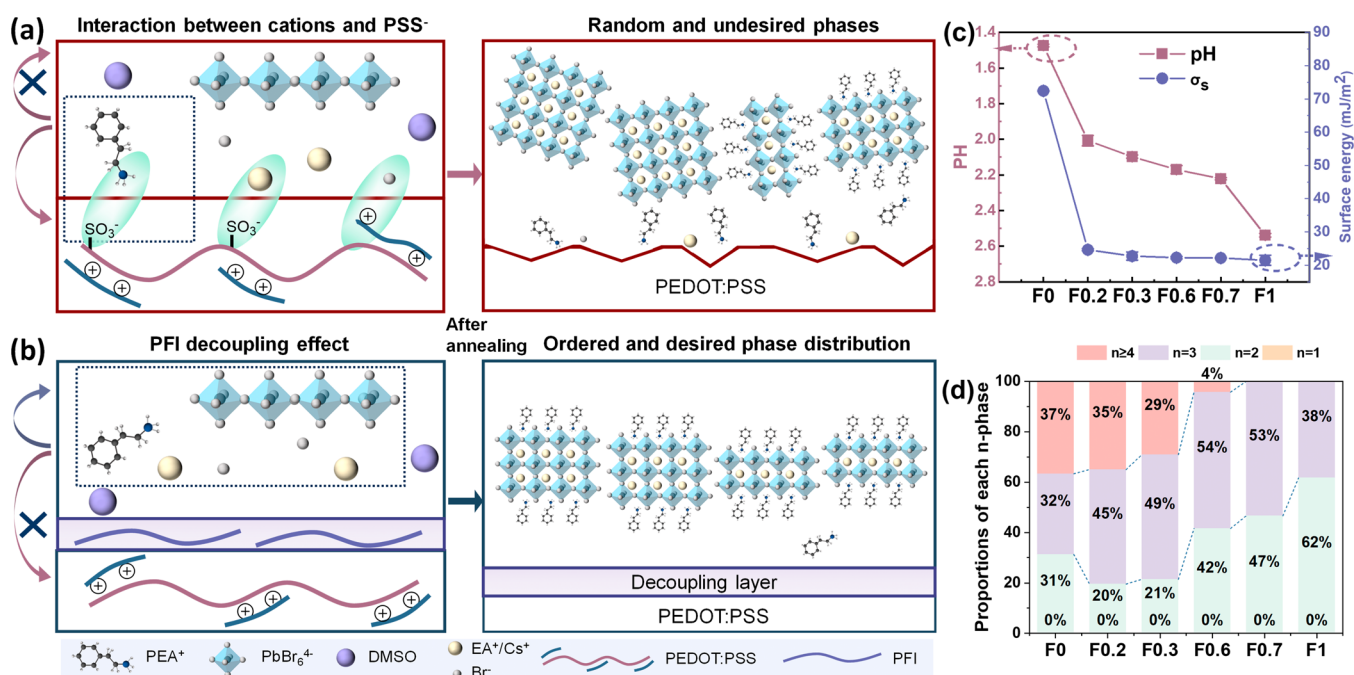


Figure 1. (a,b) Schematic illustration of how substrate influences the crystallization of quasi-2D perovskite. (c) Corresponding pH of PEDOT:PSS and surface energy of HIL films vs the PFI:PEDOT ratio. (The Owens–Wendt–Rabel–Kaelble model for calculating surface energy at ~ 25 °C and $\sim 15\%$ relative humidity, using water and diiodomethane solvents.) (d) The relative contents of different n phases for perovskite films prepared on PEDOT:PSS (AI4083) with different concentrations of PFI.

quality.^{11–13} In particular, the high density of phase impurity in perovskite on the prevalent poly(3,4-ethylenedioxythiophene):poly(styrenesulfonate) (PEDOT:PSS) substrates becomes a critical challenge for blue-emission quasi-2D PeLEDs, despite its advantages of high hole injection capability and film reproducibility.^{14,15} While the previous several studies^{16–19} have laid a valuable groundwork, a more thorough investigation on the behind mechanism is still lacking. To realize the controllable growth of phases in films, we need to gain deep insight into the interaction at the buried interface.

Addressing these challenges, we elucidate the detailed mechanisms of the interplay between substrates and quasi-2D perovskites. The large amount of sulfonate group ($-\text{SO}_3^-$) in PEDOT:PSS increases the nucleation barrier of the desired low- n phase, resulting in low-energy photon emission and hindering blue emission. Perfluorinated ionomer (PFI) in PEDOT:PSS is implemented as a decoupling layer to increase the proportion of the target phase. The photoluminescence (PL) peak blue shifts from 501.71 to 491.14 nm without incorporating Cl ions, which has been often used to achieve blue emission but can cause halide segregation issues degrading color purity. Then, the results of X-ray photoelectron spectroscopy (XPS) and Fourier transform infrared spectroscopy (FTIR) demonstrate that the buried interface alterations affect both the organic terminal layer formation (i.e., large organic cation layer) and its interaction with $[\text{PbBr}_6]^{4-}$ octahedral units within the quantum-well-type perovskite. In addition, the Grazing-incidence wide-angle X-ray scattering (GIWAXS) results verified the improved crystallinity and ordered grain orientation, while time-resolved photoluminescence (TRPL) and photoluminescence quantum yield (PLQY) results confirmed reduced defect-induced nonradiative recombination losses. As a result, the PFI-based

device displayed the highest peak (external quantum efficiency) EQE of 12.09%.

The growth mechanism of quasi-2D perovskites is associated with the formation of intermediate complexes during the annealing process, enabling lattice expansion, reagent infiltration and organic bilayer nucleation in reduced-dimensional perovskites (RDPs) films (“organic bilayers” refer to PEA combining with octahedral to generate a small unit with $n = x$).²⁰ The comprehensive growth mechanism should be expanded, especially on the interaction between substrates and precursors, which has been neglected but is crucial for crystallization. Here, a mechanistic model was first used to depict QW formation at the hole injection layer (HIL)/quasi-2D perovskite interface.

Figure 1a illustrates the dynamic change in the formation process of the organic double layer as PEA is consumed and redistributed during QW growth. With the presence of dimethyl sulfoxide (DMSO), PEA^+ ions undergo solvation and recrystallization, combining with other anions through electrostatic interactions. On the other hand, the thermal annealing facilitates the deprotonation reaction of $-\text{SO}_3\text{H}$ within PEDOT:PSS to produce $-\text{SO}_3^-$, as shown in reaction formula 1. This reaction increases PEA^+ consumption through combination with $-\text{SO}_3^-$, as shown in reaction formula 2. The depletion of PEA^+ induced by PEDOT:PSS weakens control over perovskite crystal growth, increasing the propensity for the formation of high- n phase domains. If this strong depletion of organic cations can be suppressed to promote formation of an organic bilayer, the probability of low- n phase generation can be increased.

Herein, PFI was introduced as a decoupling layer between PEDOT:PSS and perovskites and could self-organize into a stable interfacial top surface layer due to its lower fluorocarbon surface energy.²¹ Figure 1b illustrates how PFI acts as a barrier, preventing the interaction between organic cations and

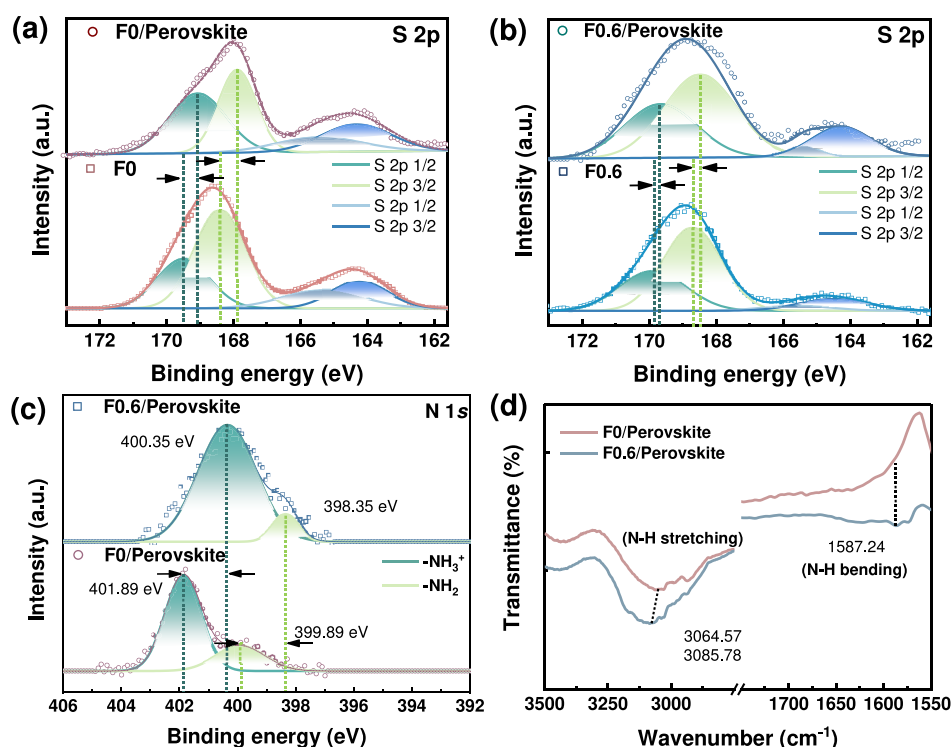
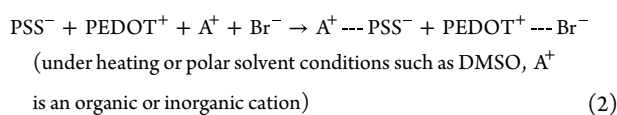
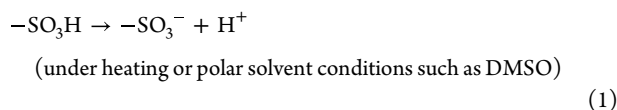


Figure 2. XPS spectra of S 2p prepared in (a) F0 and (b) F0.6 with or without perovskite films. (c) XPS spectra of N 1s and (d) characteristic FTIR absorption peak of NH_3^+ of perovskite films.

abundant $-\text{SO}_3\text{H}$ content. PFI reduces local organic cation depletion, allowing freer diffusion of PEA^+ cations to interact with inorganic octahedral monolayers $[\text{PbBr}_6]^{4-}$. This promotes the formation of RDP crystallites, which in turn suppress undesired phase formation.



To verify how the substrate affects phase distribution in blue quasi-2D perovskite layers, $\text{PEA}_2(\text{EA}_{0.6}\text{Cs}_{0.4})_{n-1}\text{Pb}_3\text{Br}_{10}$ ($n = 3$) was fabricated without incorporating additional additives or passivation agents as the emitting layer (EML). PFI was systematically introduced into PEDOT:PSS at varying concentrations, corresponding to F0, F0.2, F0.3, F0.6, F0.7, and F1. As shown in Figure 1c, the acidity of HIL solution decreased with higher PFI ratios due to the decreased concentration of dissociated $-\text{SO}_3\text{H}$ in water. And the surface energy (SFE) of the PEDOT:PSS substrate also decreased, attributed to the vertical self-organization of highly hydrophobic PFI on surface.²² These results indicate the efficient decoupling effect of PFI, which could decrease the number of $-\text{SO}_3\text{H}$ surface terminals.

Moreover, the increased SFE by introducing PFI led to a blue-shifted PL peak, as evidenced in Figure S1a,b. The ultraviolet–visible (UV–vis) absorption spectrum (Figure S1c,d) confirmed that the introduction of PFI could induce more low- n phase ($n = 2, 3$). The second derivative of the ultraviolet–visible (UV–vis) absorption spectrum was em-

ployed to resolve the characteristic peaks for different phases,²³ and integrated areas quantified relative phase distribution in quasi-2D perovskites (Figure 1d and Figure S2). As PFI increased, the relative absorption intensity of the low- n phase ($n = 2, 3$) perovskite content increased. Above results were consistent with our proposed mechanism (Figure 1a,b), demonstrating that the decoupling layer can effectively hinder the formation of an undesired phase in quasi-2D perovskites.

To get a deep understanding of the interface interaction, we post-treated the substrates with dilute perovskite precursors to build a 10 nm perovskite film and then employed XPS and Raman spectroscopy to trace elemental variations. The typical C 1s peak of PEDOT:PSS with or without PFI is shown in Figure S3.^{21,22} In addition to the $-\text{CF}_3$ (at ~ 293 eV) and $-\text{CF}_2$ (at ~ 291.3 eV) peaks from C 1s, a single peak (at 688.25 eV) from F 1s is also associated with PFI, indicating that PFI is dispersed on the PEDOT:PSS surface. In addition, sulfur (S) peaks at 168.6 and 164.3 eV in Figure 2a,b correspond to the S atom signals from PSS and PEDOT, respectively. After perovskite precursor flushing, the shift of sulfur atom signals from PSS was observed. The shift is caused by the combination of sulfur with positively charged cations such as PEA^+ , EA^+ or Cs^+ in perovskite precursors, which induce a screening effect and decreases the interaction between PSS and PEDOT chains, accelerating their separation.²⁴ Notably, PFI on PEDOT:PSS can inhibit the shift of the sulfur atom signals. Raman spectra (Figure S4) show that the symmetric $\text{C}\alpha=\text{C}\beta$ stretching vibrations (~ 1452 cm^{-1}) of the thiophene ring in PEDOT:PSS shift by 14.13 cm^{-1} without PFI.²⁵ In contrast, with PFI, this shift is reduced to a 7.85 cm^{-1} shift. These results indicate the decoupling effect of PFI, reducing cation consumption and improving experiment repeatability.²⁶

Further, a combination of XPS and FTIR was employed to trace elemental variation on different buried interfaces. As

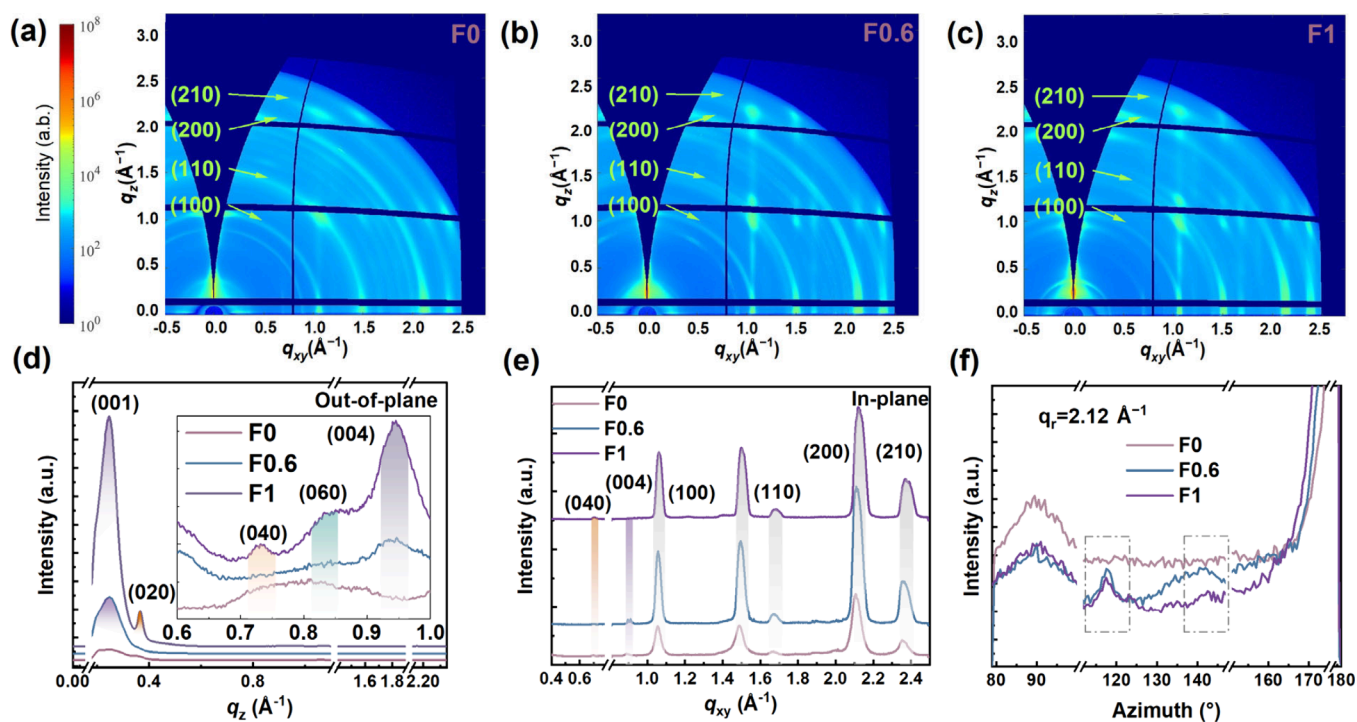


Figure 3. (a–c) GIWAXS patterns for the perovskite films on different substrates. (d) Out-of-plane and (e) in-plane diffraction pattern. (f) Integrated intensity plots azimuthally along the ring at q_r approximate to 2.12 \AA^{-1} , assigned to the (200) $n = \infty$ phase.

depicted in Figure 2c, the binding energy (BE) of N 1s in perovskite films on F0.6 (400.4 eV) was lower than that on F0 (401.9 eV). The change can be attributed to the less formation of uncoordinated $-\text{NH}_3^+$ sites and enhanced interaction of $-\text{NH}_3^+$ with $[\text{PbBr}_6]^{4-}$ complexes in perovskite on F0.6.²⁷ The increased N/Pb ratio of perovskite on F0.6 (from 0.123 to 0.141) also proves the strong affinity of $-\text{NH}_3^+$ ions with the $[\text{PbBr}_6]^{4-}$ octahedron.^{28,29} In Figure 2d, the $-\text{NH}_3^+$ peak in perovskite shifting to a longer wavelength on F0.6 implied that intermolecular interactions within the perovskite material have strengthened, due to the strengthening hydrogen bonds or an increase in intermolecular electrostatic forces.^{30,31} This leads to a more stable and well-defined perovskite QW architecture, which enhances its optoelectronic properties.

The Cs 3d and Pb 4f core levels vary with different substrates, suggesting that the substrates affects the CsPbBr₃ crystal structure rather than merely the surface terminated PEA^+ (Figure S5a,b).³² The Cs 3d peaks on F0.6 shift to lower energy compared to those on F0, indicating reduced uncoordinated Cs⁺ sites in perovskite on F0.6.³³ Additionally, the binding energy of the Pb 4f peak increased for perovskite on F0.6, indicating a decreased concentration of unsaturated lead and a more stable lead environment for $[\text{PbBr}_6]^{4-}$ octahedra.³⁴ The analysis of bromine (Br) sheds light on its role in modifying the bandgap in Figure S5c. The Br 3d peak shifts to higher energy on F0.6 compared to F0, attributed to changes in Pb–Br bond lengths and lattice constants of perovskite,³⁵ thereby affecting the bandgap and PL peaks.³⁶ Furthermore, the Br/Pb ratio is higher in perovskite films on F0.6 (0.269) compared to PEDOT:PSS (0.237), suggesting that PFI suppresses halide vacancy formation.³⁷

To confirm the effect of substrate surface properties on the phase formation, crystal structure, and crystal orientation in 2D perovskite films, GIWAXS and XRD measurements were conducted. Annular Debye Scherrer patterns (Figure 3a–c)

show that the formation of a lower- n phase perovskite is promoted by PFI, as evidenced by the emergence of peaks for $n = 1, 2, 3$. The GIWAXS pattern shows peaks for the $n = 1$ phase at $q = 0.36, 0.70 \text{ \AA}^{-1}$, and for the $n = 2$ phase at $q = 0.80 \text{ \AA}^{-1}$, along with strong diffraction signals in the z -direction on perovskite based on F0.6 (Figure 3d).^{38,39} In XRD results, the intensity of small angles corresponding to the $n = 2$ phase also increased after introducing PFI (Figure S6a,b).⁴⁰ As well, the increased peak intensity (at $q = 0.24, 0.91 \text{ \AA}^{-1}$) corresponding to the $n = 3$ phase³ demonstrated that the introduction of PFI could promote the formation of desired low- n phases in blue quasi-2D perovskite films.

The GIWAXS pattern displays an enhanced diffraction peak intensity and a lowered full width at half-maximum (fwhm) of the diffraction peak in perovskite films on F0.6 and F1 (Figure 3e and Table S1). This indicates that the quasi-2D perovskites have increased crystallinity and enlarged the 3D domain size with the introduction of PFI.⁴¹ Furthermore, the peak of (100) shifts to higher q for the perovskite on PEDOT:PSS with PFI (Figure 3e), suggesting a tighter crystal stacking⁴² and more stable structure,⁴³ which agrees with the Pb 4f and Br 3d XPS results.

The GIWAXS patterns ($q = 1.49\text{--}2.10 \text{ \AA}^{-1}$) show continuous uniform rings, indicating a random crystal orientation for pure PEDOT:PSS^{44,45} (Figure 3a). But with PFI introduction, the diffraction mottling at the azimuth angles of 62° ($180 - 62^\circ$) and 38° ($180 - 38^\circ$) became more obvious (Figure 3f). In addition, preferential face-on orientation in the $n = 3$ phase (Figure S7a,b) was observed, which indicates the ordered crystal orientation with the introduction of PFI in substrate.⁴⁶ Additionally, Figure S8 shows a homogeneous longitudinal distribution of perovskite, suggesting that the effect of the substrate on the phase distribution was throughout the perovskite film.

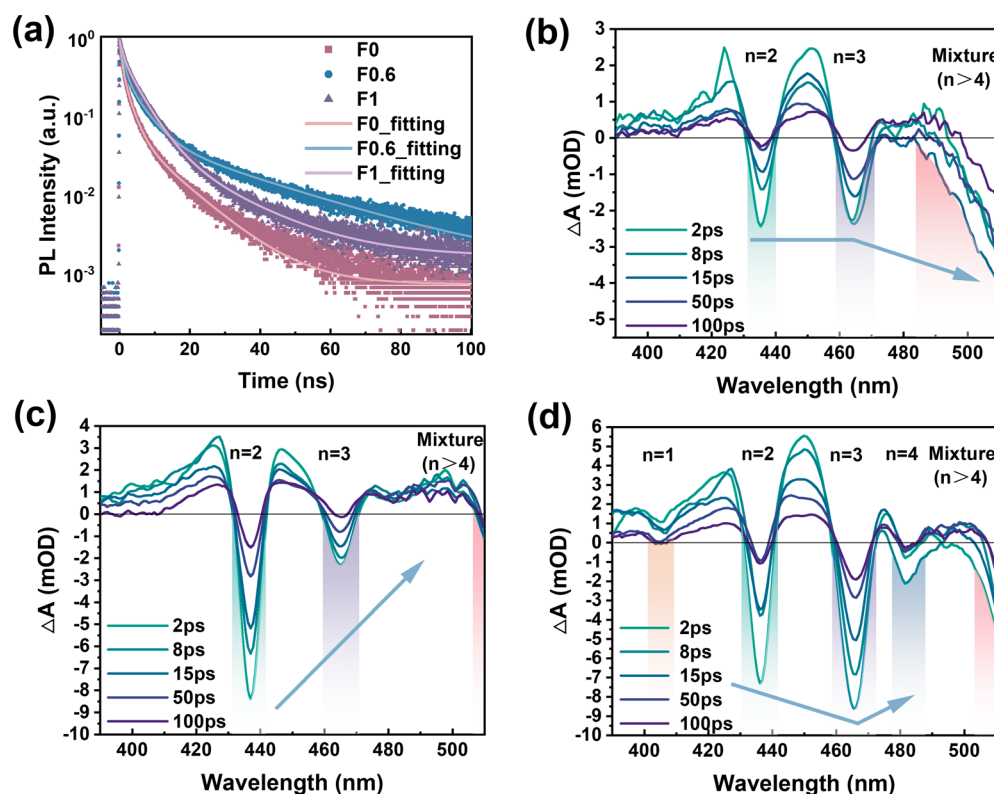


Figure 4. (a) The TRPL decay profiles of perovskite fabricated on PEDOT:PSS with different concentrations of PFI. TA spectroscopy: Time-wavelength-dependent TA at different probe delay times of perovskite on (b) F0, (c) F0.6, and (d) F1 substrates.

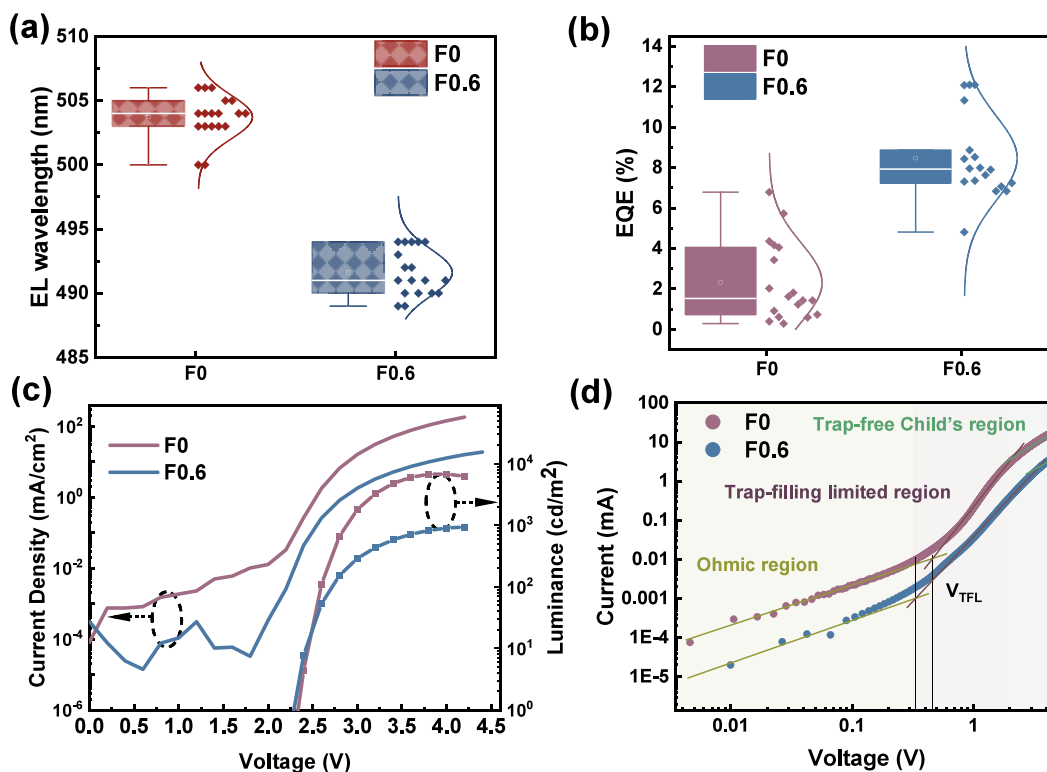


Figure 5. Effect of PEDOT:PSS with or without PFI on (a) EL wavelength distribution, (b) EQE distribution, and (c) current density–voltage–luminance (J – V – L) characteristic curves of quasi-2D PeLEDs. (d) J – V curves for SCLC test with hole-only devices based on PEDOT:PSS with or without PFI.

Following that, the influence of the substrate surface property on the formed 2D perovskite films was investigated

to strengthen the perovskite formation mechanism. In Figure S9, with the introduction of PFI, PLQY of perovskite films was

increased, suggesting an alteration in the number of 2D perovskites monolayers and reduced defects. TRPL decay profiles were measured (Figure 4a and Figure S10), and the results were fitted by triexponential decays (Table S2). Three components include efficient hole transfer from perovskite to HTL (τ_1), the defect-trapping (τ_2) and radiative recombination (τ_3).⁴⁷ It is noteworthy that films on F0.6 and F1 showed longer average TRPL lifetimes (τ_{avg}). And the longer τ_3 component in the TRPL decay is directly correlated with the observed increase in PLQY, which represents enhanced radiative recombination efficiency. This enhancement results from the formation of lower- n phases ($n = 2, 3$) with strong quantum confinement effects generated in the perovskites.⁴⁸ In addition, reduced nonradiative losses by suppressing defects at grain boundaries and interfaces during energy-funneling is also attributed to it. PFI plays a key role by promoting the formation of larger grain sizes and well-ordered, oriented perovskite films, which effectively reduce defects.

Following, transient absorption (TA) spectroscopy in Figure 4b,c and Figure S11 was used to reveal excitonic absorption bands. The observed negative spectroscopic features and positive photo-induced absorption signals correspond to ground-state bleaching (GSB) bands and excited-state absorption (ESA) spectra, respectively. Notably, the introduction of PFI into PEDOT:PSS selectively suppresses the high- n phase, preferentially facilitating smaller- n phases, as evidenced by the GSB around 500 nm. The observed increase in the $n = 2, 3$ phases upon PFI addition coincides with XRD and GIWAXS measurements (Figure S6 and Figure 3). This increased low-dimensional phase also changes the morphology of the films. The slender, flake-like grains on PFI-enriched PEDOT:PSS surfaces were observed in SEM images (Figure S12) and AFM images (Figure S13). This demonstrates that the interfacial decoupling layer alters the phase distribution within the film, hence, changing the surface morphology.

Then, devices were fabricated to evaluate the PeLEDs performance, as illustrated in Figure S14. After the introduction of PFI, the EL peak blue-shifted from 503.72 to 491.61 nm even without incorporating Cl ions (Figure 5a and Figure S15), verifying that the HIL surface effectively controls phase formation of EML. And the average EQE of devices with PFI showed a 4-fold increase (from 2.31% to 8.46%) with a peak EQE of 12.09% at 494 nm (Figure 5b). This improvement is attributed to the interface-engineered phase distribution, which minimizes impurity phase formation and results in a more ordered and uniform phase distribution within the quasi-2D perovskite film, thereby enhancing radiative recombination efficiency. In addition, the device with PFI had a decreased leakage current density at low-bias (<2.5 V) and higher brightness (Figure 5c). It should be determined by the exciton quenching blocking and the hole injection capabilities of PFI at the buried interface, which improved exciton formation and utilization efficiency.⁴⁹ Space-charge limited current (SCLC) measurements was used by fabricating the hole-only devices in Figure S16. As shown in Figure 5d and Table S3, the hole trap densities N_t based on the F0.6 devices ($2.89 \times 10^{17} \text{ cm}^{-3}$) were lower than N_t based on PEDOT:PSS ($4.01 \times 10^{17} \text{ cm}^{-3}$), indicating PFI interface effectively suppresses the formation of hole traps in PeLEDs.

The reduction of trap-assisted recombination losses and ion migration in the F0.6 device is further supported by impedance spectroscopy (IS) results. The corresponding equivalent circuit was applied^{50,51} to model the recombination resistance at

interfaces and within the perovskite material (Figure S17a and Table S4). Importantly, recombination resistances are larger for the PFI-based device, which indicates fewer defects and thus less nonradiative recombination at the HIL–perovskite interface.^{52,53} Additionally, ion migration is revealed by capacitance–frequency (C – f) curves (Figure S17b). In the low-frequency domain, devices incorporating PFI exhibit insignificant capacitance increases, indicating that the ion migration is suppressed.⁵⁴ This would enhance the stability of the perovskite film, leading to improved efficiency and long-term stability. As shown in Figure S17c,d, the operational lifetime of device increased from 1.66 to 1.9 h after using decoupling layer.

This study highlights the critical role of the substrate in the growth mechanisms in blue quasi-2D perovskites. A formation kinetics model before and after thermal annealing was used to study the formation of quantum wells and n -phase distributions at the PEDOT:PSS/perovskite interface. And PFI also forms an interfacial decoupling layer, acting as a barrier that inhibits PEA^+ from interacting with the $-\text{SO}_3\text{H}$ groups in PEDOT:PSS, allowing more PEA^+ to interact with $[\text{PbBr}_6]^{4-}$. This effectively promotes low- n phase formation and suppresses high- n phases. The refined control of phase formation facilitates radiative recombination, resulting in increased quantum yield and extended TRPL lifetimes. Consequently, the PFI-based device achieves a 4-fold increase in EQE, with a peak of 12.09%. This study not only uncovers the complex interplay between substrate properties and phase distribution but also offers new insights into enhancing their efficiency in practical applications.

■ ASSOCIATED CONTENT

Supporting Information

The Supporting Information is available free of charge at <https://pubs.acs.org/doi/10.1021/acseenergylett.4c02351>.

Experimental section (including materials, preparation of perovskite solution, fabrication of PeLEDs and characterization), additional characterization data (PL, UV–vis, XPS, Raman, XRD, GIWAXS, PLQY, TA spectra, SEM, AFM and device performance of PeLEDs) (Figures S1–S17), and Tables S1–S4 listing fwhm, PL decay lifetime, and the fitting parameters for each experiment (PDF)

■ AUTHOR INFORMATION

Corresponding Author

Tae-Woo Lee – Department of Materials Science and Engineering, Seoul National University, Seoul 08826, Republic of Korea; Institute of Engineering Research, Research Institute of Advanced Materials and Soft Foundry, Interdisciplinary Program in Bioengineering, Seoul National University, Seoul 08826, Republic of Korea; [SN Display Co., Ltd., Seoul 08826, Republic of Korea](http://www.snl.co.kr); orcid.org/0000-0002-6449-6725; Email: twlees@snu.ac.kr, taewlees@gmail.com

Authors

Jie Dong – Department of Materials Science and Engineering, Seoul National University, Seoul 08826, Republic of Korea; Key Laboratory of Luminescence and Optical Information, Ministry of Education, Institute of Optoelectronics Technology, Beijing Jiaotong University, Beijing 100044, P. R.

China; Department of Electronics & Information Engineering, Suzhou Vocational University, Suzhou, Jiangsu 215104, P. R. China

Wenqiang Yang – Department of Materials Science and Engineering, Seoul National University, Seoul 08826, Republic of Korea; Institute of Atomic Manufacturing, International Institute for Interdisciplinary and Frontiers, Beihang University, Beijing 100191, P. R. China

Kayoung Cho – Department of Chemistry and NanoScience, Ewha Womans University, Seoul 03760, Republic of Korea

Jeong Hyun Jung – Department of Materials Science and Engineering, Seoul National University, Seoul 08826, Republic of Korea

HuanYu Zhou – Department of Materials Science and Engineering, Seoul National University, Seoul 08826, Republic of Korea

Eojin Yoon – Department of Materials Science and Engineering, Seoul National University, Seoul 08826, Republic of Korea

Hao Chen – Department of Materials Science and Engineering, Seoul National University, Seoul 08826, Republic of Korea; College of Materials Science and Optoelectronic Technology, Center of Materials Science and Optoelectronics Engineering, College of Resources and Environment, CAS Center for Excellence in Topological Quantum Computation, CAS Key Laboratory of Vacuum Physic, University of Chinese Academy of Sciences, Beijing 100049, P. R. China

Hyeon-Dong Lee – Department of Materials Science and Engineering, Seoul National University, Seoul 08826, Republic of Korea

Seung Hyeon Jo – Department of Materials Science and Engineering, Seoul National University, Seoul 08826, Republic of Korea

Jae-Man Park – Department of Materials Science and Engineering, Seoul National University, Seoul 08826, Republic of Korea; Institute of Engineering Research, Research Institute of Advanced Materials, Seoul National University, Seoul 08826, Republic of Korea

Qingsen Zeng – Department of Materials Science and Engineering, Seoul National University, Seoul 08826, Republic of Korea

Tingyu Long – Department of Materials Science and Engineering, Seoul National University, Seoul 08826, Republic of Korea

Kyung Yeon Jang – Department of Materials Science and Engineering, Seoul National University, Seoul 08826, Republic of Korea

Seong Eui Chang – Department of Materials Science and Engineering, Seoul National University, Seoul 08826, Republic of Korea; orcid.org/0009-0004-5554-0626

Chan-Yul Park – Department of Materials Science and Engineering, Seoul National University, Seoul 08826, Republic of Korea

Min-Jun Sung – Department of Materials Science and Engineering, Seoul National University, Seoul 08826, Republic of Korea

Joo Sung Kim – Department of Materials Science and Engineering, Seoul National University, Seoul 08826, Republic of Korea

Hyeeree Kim – Department of Materials Science and Engineering, Seoul National University, Seoul 08826, Republic of Korea

Dandan Song – Key Laboratory of Luminescence and Optical Information, Ministry of Education, Institute of Optoelectronics Technology, Beijing Jiaotong University, Beijing 100044, P. R. China; orcid.org/0000-0002-5050-8211

Zheng Xu – Key Laboratory of Luminescence and Optical Information, Ministry of Education, Institute of Optoelectronics Technology, Beijing Jiaotong University, Beijing 100044, P. R. China; orcid.org/0000-0001-9680-2208

JaeHong Park – Department of Chemistry and NanoScience, Ewha Womans University, Seoul 03760, Republic of Korea; orcid.org/0000-0002-0509-3934

Jeong-Yun Sun – Department of Materials Science and Engineering, Seoul National University, Seoul 08826, Republic of Korea; Institute of Engineering Research, Research Institute of Advanced Materials, Seoul National University, Seoul 08826, Republic of Korea; orcid.org/0000-0002-7276-1947

Complete contact information is available at:

<https://pubs.acs.org/10.1021/acsenerylett.4c02351>

Notes

The authors declare no competing financial interest.

ACKNOWLEDGMENTS

This work was supported by the National Research Foundation of Korea (NRF) grant funded by the Korean government (Ministry of Science, ICT & Future Planning) (NRF-2016R1A3B1908431). And this work was also supported by the Technology Innovation Program Development Program (00235080) funded by the Ministry of Trade, Industry & Energy (MOTIE, Korea).

REFERENCES

- (1) Cai, W.; Ali, M. U.; Liu, P.; He, M.; Zhao, C.; Chen, Z.; Zang, Y.; Tang, M.-C.; Meng, H.; Fu, H.; et al. Unravelling Alkali-Metal-Assisted Domain Distribution of Quasi-2D Perovskites for Cascade Energy Transfer toward Efficient Blue Light-Emitting Diodes. *Adv. Sci.* **2022**, *9* (20), 2200393.
- (2) Zhang, F.; Gao, Y.; Wang, D.; Lu, P.; Wang, X.; Lu, M.; Wu, Y.; Chen, P.; Hu, J.; Bai, X.; et al. Phase Distribution Management for High-Efficiency and Bright Blue Perovskite Light-Emitting Diodes. *Nano Energy* **2024**, *120*, 109144.
- (3) Wang, C.; Dai, G.; Wang, J.; Cui, M.; Yang, Y.; Yang, S.; Qin, C.; Chang, S.; Wu, K.; Liu, Y.; et al. Low-Threshold Blue Quasi-2D Perovskite Laser through Domain Distribution Control. *Nano Lett.* **2022**, *22* (3), 1338–1344.
- (4) Coffey, A. H.; Yang, S. J.; Gómez, M.; Finkenauer, B. P.; Terlier, T.; Zhu, C.; Dou, L. Controlling Crystallization of Quasi-2D Perovskite Solar Cells: Incorporating Bulky Conjugated Ligands. *Adv. Energy Mater.* **2023**, *13* (33), 2201501.
- (5) Chen, P.; Meng, Y.; Ahmadi, M.; Peng, Q.; Gao, C.; Xu, L.; Shao, M.; Xiong, Z.; Hu, B. Charge-Transfer versus Energy-Transfer in Quasi-2D Perovskite Light-Emitting Diodes. *Nano Energy* **2018**, *50*, 615–622.
- (6) Liu, Y.; Yu, Z.; Chen, S.; Park, J. H.; Jung, E. D.; Lee, S.; Kang, K.; Ko, S.-J.; Lim, J.; Song, M. H.; et al. Boosting The Efficiency of Quasi-2D Perovskites Light-Emitting Diodes by Using Encapsulation Growth Method. *Nano Energy* **2021**, *80*, 105511.
- (7) Fakharuddin, A.; Gangishetty, M. K.; Abdi-Jalebi, M.; Chin, S.-H.; bin Mohd Yusoff, A. R.; Congreve, D. N.; Tress, W.; Deschler, F.; Vasilopoulou, M.; Bolink, H. J. J. N. E. Perovskite Light-Emitting Diodes. *Nat. Electron.* **2022**, *5* (4), 203–216.

- (8) Liu, S.; Guo, Z.; Wu, X.; Liu, X.; Huang, Z.; Li, L.; Zhang, J.; Zhou, H.; Sun, L.-D.; Yan, C.-H. Zwitterions Narrow Distribution of Perovskite Quantum Wells for Blue Light-Emitting Diodes with Efficiency Exceeding 15. *Adv. Mater.* **2023**, *35* (3), 2208078.
- (9) Pang, P.; Jin, G.; Liang, C.; Wang, B.; Xiang, W.; Zhang, D.; Xu, J.; Hong, W.; Xiao, Z.; Wang, L.; et al. Rearranging Low-Dimensional Phase Distribution of Quasi-2D Perovskites for Efficient Sky-Blue Perovskite Light-Emitting Diodes. *ACS Nano* **2020**, *14* (9), 11420–11430.
- (10) Zhang, X.; Munir, R.; Xu, Z.; Liu, Y.; Tsai, H.; Nie, W.; Li, J.; Niu, T.; Smilgies, D.-M.; Kanatzidis, M. G.; et al. Phase Transition Control for High Performance Ruddlesden–Popper Perovskite Solar Cells. *Adv. Mater.* **2018**, *30* (21), 1707166.
- (11) Guan, Z.; Shen, D.; Li, M.; Ma, C.; Chen, W.-C.; Cui, X.; Liu, B.; Lo, M.-F.; Tsang, S.-W.; Lee, C.-S.; et al. Effects of Hydrogen Bonds between Polymeric Hole-Transporting Material and Organic Cation Spacer on Morphology of Quasi-Two-Dimensional Perovskite Grains and Their Performance in Light-Emitting Diodes. *ACS Appl. Mater. Interfaces* **2020**, *12* (8), 9440–9447.
- (12) Xing, J.; Zhao, Y.; Askerka, M.; Quan, L. N.; Gong, X.; Zhao, W.; Zhao, J.; Tan, H.; Long, G.; Gao, L.; et al. Color-Stable Highly Luminescent Sky-Blue Perovskite Light-Emitting Diodes. *Nat. Commun.* **2018**, *9* (1), 3541.
- (13) Zeng, J.; Sun, X.; Liu, Y.; Jin, W.; He, S.; Zhu, X.; Niu, K.; Sun, G.; Li, J.; He, H.; et al. Switchable Interfacial Reaction Enables Bright and Stable Deep-Red Perovskite Light-Emitting Diodes. *Nat. Photonics* **2024**, *18* (4), 325–333.
- (14) Wang, Y.; Xu, Y.; Yun, J.; Cai, Q.; Zhai, L.; Zhuang, D.; Yang, G.; Huang, H.; Li, M.; Yang, Y.; et al. Suppressing Interfacial Nonradiative Recombination by Alkali Hydroxides for Efficient Blue Perovskite Light-Emitting Diodes. *Chem. Eng. J.* **2024**, *486*, 149964.
- (15) Xu, L.; Wu, Z.; Jiang, C.; Liu, M.; Li, B.; Lin, H.; Liu, W.; Peng, H.; Luo, C. Low-Dimensional Phase Distribution of Quasi-2D Perovskites Induced by Interfacial Effect Enables Efficient Blue Light-Emitting Diodes. *Adv. Opt. Mater.* **2024**, *12* (4), 2301615.
- (16) Li, H.; Wu, J.; Hu, S.; Zhang, W.; Gao, J.; Guo, Y.; Guo, P.; Liu, C.; Zhao, G.; Fu, M. J. A. F. M. Air-Processed Blue Perovskite Light-Emitting Diodes Enabled by Manipulation of Adsorbed-Moisture-Dominated Crystallization Kinetics. *Adv. Funct. Mater.* **2023**, *33* (44), 2303787.
- (17) Liu, L.; Dong, R.; Ge, H.; Piao, J.; Wang, Y.; Li, S.; Shen, W.; Cao, K.; Chen, S. Basic Amino Acids Modulated Neutral-pH PEDOT:PSS for Stable Blue Perovskite Light-Emitting Diodes. *ACS Appl. Mater. Interfaces* **2022**, *14* (24), 28133–28144.
- (18) Chu, Z.; Zhang, W.; Jiang, J.; Qu, Z.; Ma, F.; Zhao, Y.; Chu, X.; Shen, Y.; Li, Y.; Yin, Z.; et al. Blue Light-Emitting Diodes Based on Quasi-Two-Dimensional Perovskite with Efficient Charge Injection and Optimized Phase Distribution via An Alkali Metal Salt. *Nat. Electron.* **2023**, *6* (5), 360–369.
- (19) Seop Shin, Y.; Jin Yoon, Y.; Hyeon Kweon, S.; Hak Oh, S.; Beom Park, C.; Yuk, D.; Song, T.; Geon Son, J.; Seo, J.; Lee, W.; et al. Controlling The Formation Energy of Perovskite Phase via Surface Polarity of Substrate for Efficient Pure-Blue Light-Emitting Diodes. *Chem. Eng. J.* **2023**, *464*, 142707.
- (20) Quintero-Bermudez, R.; Gold-Parker, A.; Proppe, A. H.; Munir, R.; Yang, Z.; Kelley, S. O.; Amassian, A.; Toney, M. F.; Sargent, E. H. Compositional and Orientational Control in Metal Halide Perovskites of Reduced Dimensionality. *Nat. Mater.* **2018**, *17* (10), 900–907.
- (21) Lee, T.-W.; Chung, Y.; Kwon, O.; Park, J.-J. Self-Organized Gradient Hole Injection to Improve the Performance of Polymer Electroluminescent Devices. *Adv. Funct. Mater.* **2007**, *17* (3), 390–396.
- (22) Jeong, S.-H.; Woo, S.-H.; Han, T.-H.; Park, M.-H.; Cho, H.; Kim, Y.-H.; Cho, H.; Kim, H.; Yoo, S.; Lee, T.-W. Universal High Work Function Flexible Anode for Simplified ITO-Free Organic and Perovskite Light-Emitting Diodes with Ultra-High Efficiency. *Npg Asia Mater.* **2017**, *9* (7), e411–e411.
- (23) Wang, K.; Lin, Z. Y.; Zhang, Z.; Jin, L.; Ma, K.; Coffey, A. H.; Atapattu, H. R.; Gao, Y.; Park, J.-Y.; Zitang, Wei; et al. Suppressing phase disproportionation in quasi-2D perovskite light-emitting diodes. *Nat. Commun.* **2023**, *14* (1), 397.
- (24) Wu, X.; Wu, D.; Cui, G.; Jiang, Z.; Zhao, C.; Tang, X.; Dong, X.; Liu, N.; Zuo, Z.; Kong, L. J. S. R. Exceeding 20% Efficiency for Highly Efficient and Stable Inverted Perovskite Solar Cells via Sodium Borohydride Induced Interface Engineering. *Sol. RRL* **2023**, *7* (1), 2200833.
- (25) Jeong, S.-H.; Kim, H.; Park, M.-H.; Lee, Y.; Li, N.; Seo, H.-K.; Han, T.-H.; Ahn, S.; Heo, J.-M.; Kim, K. S.; et al. Ideal Conducting Polymer Anode for Perovskite Light-Emitting Diodes by Molecular Interaction Decoupling. *Nano Energy* **2019**, *60*, 324–331.
- (26) Song, D.; Li, H.; Xu, Y.; Yu, Q. Amplifying Hole Extraction Characteristics of PEDOT:PSS via Post-treatment with Aromatic Diammonium Acetates for Tin Perovskite Solar Cells. *ACS Energy Lett.* **2023**, *8* (8), 3280–3287.
- (27) Li, Y.; Wu, J.; Zhang, Y.; Zhang, L.; Zhou, X.; Hu, B.; Jiang, Z.; Zeng, J.; Wang, D.; Liu, Y.; et al. Whether Organic Spacer Cations Induced 2D/3D or Quasi-2D/3D Mixed Dimensional Perovskites? *Chem. Eng. J.* **2022**, *450*, 137887.
- (28) Wang, H.; Ye, F.; Sun, J.; Wang, Z.; Zhang, C.; Qian, J.; Zhang, X.; Choy, W. C. H.; Sun, X. W.; Wang, K.; et al. Efficient CsPbBr₃ Nanoplatelet-Based Blue Light-Emitting Diodes Enabled by Engineered Surface Ligands. *ACS Energy Lett.* **2022**, *7* (3), 1137–1145.
- (29) Jung, D. H.; Park, J. H.; Lee, H. E.; Byun, J.; Im, T. H.; Lee, G. Y.; Seok, J. Y.; Yun, T.; Lee, K. J.; Kim, S. O. J. N. E. Flash-Induced Ultrafast Recrystallization of Perovskite for Flexible Light-Emitting Diodes. *Nano Energy* **2019**, *61*, 236–244.
- (30) Zhang, F.; Cai, B.; Song, J.; Han, B.; Zhang, B.; Zeng, H. Efficient Blue Perovskite Light-Emitting Diodes Boosted by 2D/3D Energy Cascade Channels. *Adv. Funct. Mater.* **2020**, *30* (27), 2001732.
- (31) Krishnamurthi, P.; Ramalingam, H.; Raju, K. J. A. A. S. FTIR Studies of Hydrogen Bonding Interaction Between the Hydroxyl and Carbonyl Liquids. *Adv. Appl. Sci. Res.* **2015**, *6*, 44–52.
- (32) Wang, Y.; Zhang, T.; Kan, M.; Li, Y.; Wang, T.; Zhao, Y. Efficient α -CsPbI₃ Photovoltaics with Surface Terminated Organic Cations. *Joule* **2018**, *2* (10), 2065–2075.
- (33) Warby, J. H.; Wenger, B.; Ramadan, A. J.; Oliver, R. D. J.; Sansom, H. C.; Marshall, A. R.; Snaith, H. J. Revealing Factors Influencing the Operational Stability of Perovskite Light-Emitting Diodes. *ACS Nano* **2020**, *14* (7), 8855–8865.
- (34) Dong, Y.; Zhang, J.; Wang, W.; Hu, B.; Xia, D.; Lin, K.; Geng, L.; Yang, Y. Regulating Crystallization and Lead Leakage of Perovskite Solar Cell via Novel Polyoxometalate-Based Metal–Organic Framework. *Small* **2023**, *19* (29), 2301824.
- (35) Yi, N.; Wang, S.; Duan, Z.; Wang, K.; Song, Q.; Xiao, S. Tailoring the Performances of Lead Halide Perovskite Devices with Electron-Beam Irradiation. *Adv. Mater.* **2017**, *29* (34), 1701636.
- (36) Wang, Q.; Shao, Y.; Xie, H.; Lyu, L.; Liu, X.; Gao, Y.; Huang, J. Qualifying Composition Dependent p and n Self-Doping in CH₃NH₃PbI₃. *Appl. Phys. Lett.* **2014**, *105* (16), 163508.
- (37) Woo, J. Y.; Kim, Y.; Bae, J.; Kim, T. G.; Kim, J. W.; Lee, D. C.; Jeong, S. Highly Stable Cesium Lead Halide Perovskite Nanocrystals through in Situ Lead Halide Inorganic Passivation. *Chem. Mater.* **2017**, *29* (17), 7088–7092.
- (38) Jiang, N.; Wang, Z.; Zheng, Y.; Guo, Q.; Niu, W.; Zhang, R.; Huang, F.; Chen, D. 2D/3D Heterojunction Perovskite Light-Emitting Diodes with Tunable Ultrapure Blue Emissions. *Nano Energy* **2022**, *97*, 107181.
- (39) Shin, Y. S.; Park, C. B.; Adhikari, A.; Yoon, Y. J.; Cho, H. W.; Son, J. G.; Seo, J.; Song, T.; Lee, W.; Yeop, J.; et al. Manipulated Interface for Enhanced Energy Cascade in Quasi-2D Blue Perovskite Light-Emitting Diodes. *ACS Energy Lett.* **2022**, *7* (10), 3345–3352.
- (40) Shang, Y.; Li, G.; Liu, W.; Ning, Z. Quasi-2D Inorganic CsPbBr₃ Perovskite for Efficient and Stable Light-Emitting Diodes. *Adv. Funct. Mater.* **2018**, *28* (22), 1801193.
- (41) Ramadan, A. J.; Jeong, W. H.; Oliver, R. D. J.; Jiang, J.; Dasgupta, A.; Yuan, Z.; Smith, J.; Lee, J. E.; Motti, S. G.; Gough, O.; et al. The Role of the Organic Cation in Developing Efficient Green

Perovskite LEDs Based on Quasi-2D Perovskite Heterostructures. *Adv. Funct. Mater.* **2024**, *34* (14), 2309653.

(42) Zheng, X.; Wu, C.; Jha, S. K.; Li, Z.; Zhu, K.; Priya, S. Improved Phase Stability of Formamidinium Lead Triiodide Perovskite by Strain Relaxation. *ACS Energy Lett.* **2016**, *1* (5), 1014–1020.

(43) Jin, B.; Cao, J.; Yuan, R.; Cai, B.; Wu, C.; Zheng, X. J. A. E.; Research, S. Strain Relaxation for Perovskite Lattice Reconfiguration. *Adv. Energy Sus. Res.* **2023**, *4* (4), 2200143.

(44) Hoffman, J. M.; Hadar, I.; Li, X.; Ke, W.; Vasileiadou, E. S.; Strzalka, J.; Chen, L. X.; Kanatzidis, M. G. Film Formation Mechanisms in Mixed-Dimensional 2D/3D Halide Perovskite Films Revealed By in Situ Grazing-Incidence Wide-Angle X-Ray Scattering. *Chem.* **2022**, *8* (4), 1067–1082.

(45) Ramadan, A. J.; Jeong, W. H.; Oliver, R. D. J.; Jiang, J.; Dasgupta, A.; Yuan, Z.; Smith, J.; Lee, J. E.; Motti, S. G.; Gough, O.; et al. The Role of the Organic Cation in Developing Efficient Green Perovskite LEDs Based on Quasi-2D Perovskite Heterostructures. *Adv. Funct. Mater.* **2024**, *34* (14), 2309653.

(46) He, B.; Liu, T.; Wang, C.; Wen, Z.; Sun, B.; Wen, W.; Xing, G.; Gao, X.; Chen, S. Improving Crystallinity and Out-of-Plane Orientation in Quasi-2D Ruddlesden-Popper Perovskite by Fluorinated Organic Salt for Light-Emitting Diodes. *Small* **2023**, *19* (49), 2303255.

(47) Yuan, L.; Zhu, W.; Zhang, Y.; Li, Y.; Chan, C. C. S.; Qin, M.; Qiu, J.; Zhang, K.; Huang, J.; Wang, J.; et al. A Conformally Bonded Molecular Interface Retarded Iodine Migration for Durable Perovskite Solar Cells. *Energy Environ. Sci.* **2023**, *16* (4), 1597–1609.

(48) Jiang, Y.; Cui, M.; Li, S.; Sun, C.; Huang, Y.; Wei, J.; Zhang, L.; Lv, M.; Qin, C.; Liu, Y.; et al. Reducing the Impact of Auger Recombination in Quasi-2D Perovskite Light-Emitting Diodes. *Nat. Commun.* **2021**, *12* (1), 336.

(49) Wang, Q.; Chen, Y.; Yan, C.; Zeng, X.; Fu, X.; Pan, L.; Cao, J.; Yang, S.; Li, W.; Chen, X.; et al. Molecularly Designing a Passivation ETL to Suppress EQE Roll-off of PeLEDs. *ACS Energy Lett.* **2023**, *8* (9), 3710–3719.

(50) Bredar, A. R. C.; Chown, A. L.; Burton, A. R.; Farnum, B. H. Electrochemical impedance spectroscopy of metal oxide electrodes for energy applications. *ACS Appl. Energy Mater.* **2020**, *3* (1), 66–98.

(51) Yu, C.; Zhang, H.; Wang, P.; Wang, H.; Li, T.; Zhang, X.; Cheng, S.; Guo, C.; Gao, C.; Liu, D.; et al. Enhanced Efficiency and Stability of Quasi-2D Perovskite Light-Emitting Diodes with Cross-linkable Alkenyl Amine Cations. *Adv. Opt. Mater.* **2021**, *9* (24), 2101475.

(52) Iskandar, J.; Lee, C.-C.; Kurniawan, A.; Cheng, H.-M.; Liu, S.-W.; Biring, S. Improving the Efficiency of Near-IR Perovskite Leds via Surface Passivation and Ultrathin Interfacial Layers. *Cell Rep. Phys. Sci.* **2022**, *3* (12), 101170.

(53) Li, J.; Duan, C.; Wen, Q.; Yuan, L.; Zou, S.; Chen, C.; Xie, W.; Lin, D.; Chan, C. C. S.; Wong, K. S.; et al. Reciprocally Photovoltaic Light-Emitting Diode Based on Dispersive Perovskite Nanocrystal. *Small* **2022**, *18* (18), 2107145.

(54) Wang, Q.; Ding, S.; He, S.; Zhang, T.; Qian, L.; Xiao, P.; Chen, T.; Xiang, C. Improving the Operational Stability of Near-Infrared Quasi-2D Perovskite Light-Emitting Diodes by Cation Engineering. *Adv. Opt. Mater.* **2023**, *11* (1), 2201778.